IBRO Neuroscience Reports 17 (2024) 161–176

Contents lists available at ScienceDirect

IBRO Neuroscience Reports

journal homepage: www.sciencedirect.com/journal/IBRO-Neuroscience-Reports

Research Paper

Celastrol alleviates secondary brain injury following intracerebral haemorrhage by inhibiting neuronal ferroptosis and blocking blood-brain barrier disruption

Min Wei [a,b,d,1], Yi Liu [c,1], Dongsheng Li [b,d,1], Xingdong Wang [d], Xiaodong Wang [b,d], Yuping Li [a,b,d], Zhengcun Yan [d], Hengzhu Zhang [a,b,d,*]

[a] Department of Neurosurgery, Graduate School of Dalian Medical University, Dalian, China
[b] Department of Neurosurgery, The Yangzhou School of Clinical Medicine of Dalian Medical University, Yangzhou, China
[c] Department of Ultrasound, Northern Jiangsu People's Hospital Affiliated to Yangzhou University, Yangzhou, China
[d] Department of Neurosurgery, Northern Jiangsu People's Hospital Affiliated to Yangzhou University, Yangzhou, China

ARTICLE INFO

Keywords:
Celastrol
Intracerebral hemorrhage
Neuronal ferroptosis
ACSL4

ABSTRACT

Background: Following recent research advancements, an increasing level of evidence had been published to indicate that celastrol exerted a therapeutic effect on a range of nervous system diseases. This study therefore aimed to investigate the potential involvement of celastrol on ferroptosis and the blood-brain barrier disruption in intracerebral haemorrhage.

Methods: We established a rat intracerebral haemorrhage and adrenal pheochromocytoma cell (PC12) OxyHb models using an ACSL4 overexpression vector. Ferroptosis-related indices were assessed using corresponding assay kits, and immunofluorescence and flow cytometry were used to measure reactive oxygen species (ROS) levels. Additionally, quantitative PCR (qPCR) and western blot analyses were conducted to evaluate the expression of key proteins and elucidate the role of celastrol in intracerebral haemorrhage (ICH).

Results: Celastrol significantly improved neurological function scores, blood-brain barrier integrity, and brain water content in rats with ICH. Moreover, subsequent analysis of ferroptosis-related markers, such as Fe2+, ROS, MDA, and SOD, suggested that celastrol exerted a protective effect against the oxidative damage induced by ferroptosis in ICH rats and cells. Furthermore, Western blotting indicated that celastrol attenuated ferroptosis by modulating the expression levels of key proteins, including acyl-CoA synthetase long-chain family member 4 (ACSL4), glutathione peroxidase 4 (GPX4), ferritin heavy chain 1 (FTH1), and anti-transferrin receptor 1 (TFR1) both in vitro and in vivo. ACSL4 overexpression attenuated the neuroprotective effects of celastrol on ICH in vitro. Molecular docking analysis revealed that celastrol interacted with ACSL4 via the GLU107, GLN109, ASN111, and LYS357 binding sites.

Conclusions: Celastrol exerted antioxidant properties and aids in neurological recovery after stroke by suppressing ACSL4 expression during ferroptosis. As such, this drug represented a promising pharmaceutical candidate for the treatment of ICH.

1. Introduction

Intracerebral haemorrhage (ICH) is a neurosurgical emergency associated with considerable disability and mortality rates. Spontaneous ICH is a global health burden, affecting 3 million people worldwide. Further, the number of patients with this condition is projected to continue to increase as the global population ages(Li et al., 2021). In 2018, a prospective, randomised, double-blind, controlled study of ICH was conducted, with results showing that prognosis was significantly poor and the mortality rate was high with cerebral haemorrhage, regardless of the surgical clearance of hematomas(Haley et al., 2018). Numerous biochemical mechanisms have been postulated to explain the

* Correspondence to: Department of Neurosurgery, Graduate School of Dalian Medical University/ The Yangzhou School of Clinical Medicine of Dalian Medical University, No. 98 of Nantong West Road, Yangzhou, Jiangsu Province, China.
E-mail address: zhanghengzhu@sina.com (H. Zhang).
[1] Drs Min Wei, Yi Liu and Dongsheng Li contributed equally to this article.

https://doi.org/10.1016/j.ibneur.2024.08.003
Received 19 April 2024; Accepted 5 August 2024
Available online 6 August 2024

Table 1
Primer sequences designed for RT-PCR.

Gene	Forward sequence (5'-3')	Reverse sequence (5'-3')
ACSL4	CTTCCTCTTAAGGCCGGGAC	AGCCAGCAATAAAGTACACAGAT
GPx4	AATTCGCAGCCAAGGACATCG	ATTCGTAAACCACACTCGGCGTA
FTH1	GATCTGGCGGTTGATGGCAG	ATGATTCTTTGCCTGAGTTGCTT
TFR1	AAAATCCGGTGTAGGCACAG	CCTTTAAATGCAGGGACGAA
GAPDH	ACAGCAACAGGGTGGTGGAC	TTTGAGGGTGCAGCGAACTT

progressive damage following intracerebral haemorrhage, including oxidative damage, inflammation, blood-brain barrier disruption, brain oedema, and glutamate toxicity(Bai et al., 2020). Additionally, ICH has been shown to induce apoptosis or programmed cell death in neurones around the haematoma through the overexpression and dysfunction of cell death signalling pathways(Shi et al., 2019). Secondary brain damage following ICH can be further exacerbated by inflammatory reactions via blood-brain barrier disruption, brain oedema, and initiation and amplification of oxidative stress responses, thus increasing neuronal apoptosis and necrosis.

In 2012, ferroptosis was defined as a novel programmed cell death process. Dixon identified ferroptosis as a mode of iron overload-dependent accumulation of lethal lipid peroxides(Dixon et al., 2012). The ferroptosis-mediated cellular changes include glutathione (GSH) depletion, excessive accumulation of cellular lipid reactive oxygen species (ROS), decreased glutathione peroxidase 4 (GPX4), and other activated lipid metabolism regulatory molecules(Stockwell et al., 2017; Wang et al., 2021). Before ferroptosis identified, several studies had been made significant inroads toward the ferroptosis-associated biomarkers following haemorrhagic stroke (Cao et al., 2021, Duan et al., 2021). More importantly, modulation of ferroptosis in neuronal cells was proved to be a therapeutic potential for treating haemorrhagic stroke(Ren et al., 2022; Qu et al., 2021). However, experimental limitations and technological challenges indicate that several critical issues remain to be discussed and resolved. Therefore, we explored the current research of celastrol in animal models ICH through the modulation of ferroptosis.

Celastrol protects neurological functions by alleviating inflammation and oxidative stress(Jiang et al., 2018; Zhang et al., 2021a). This pentacyclic triterpenoid compound, is extracted from the roots of *Tripterygium wilfordii* Hook F (TWHF), commonly known as "Thunder God Vine" or "lei gong teng", indigenous to China(Zhang et al., 2017). Celastrol has long been used in traditional Chinese medicine to treat various diseases, and has been shown to exhibit many pharmacological activities, including anti-inflammatory, anti-autoimmune, anti-fibrosis, anti--atherosclerosis, anti-neurodegenerative, and anti-renal effects. In recent years, several studies have confirmed its protective effects against nervous system diseases, particularly its pharmacological efficacy against neurodegenerative diseases and vascular injuries. Celastrol relieves

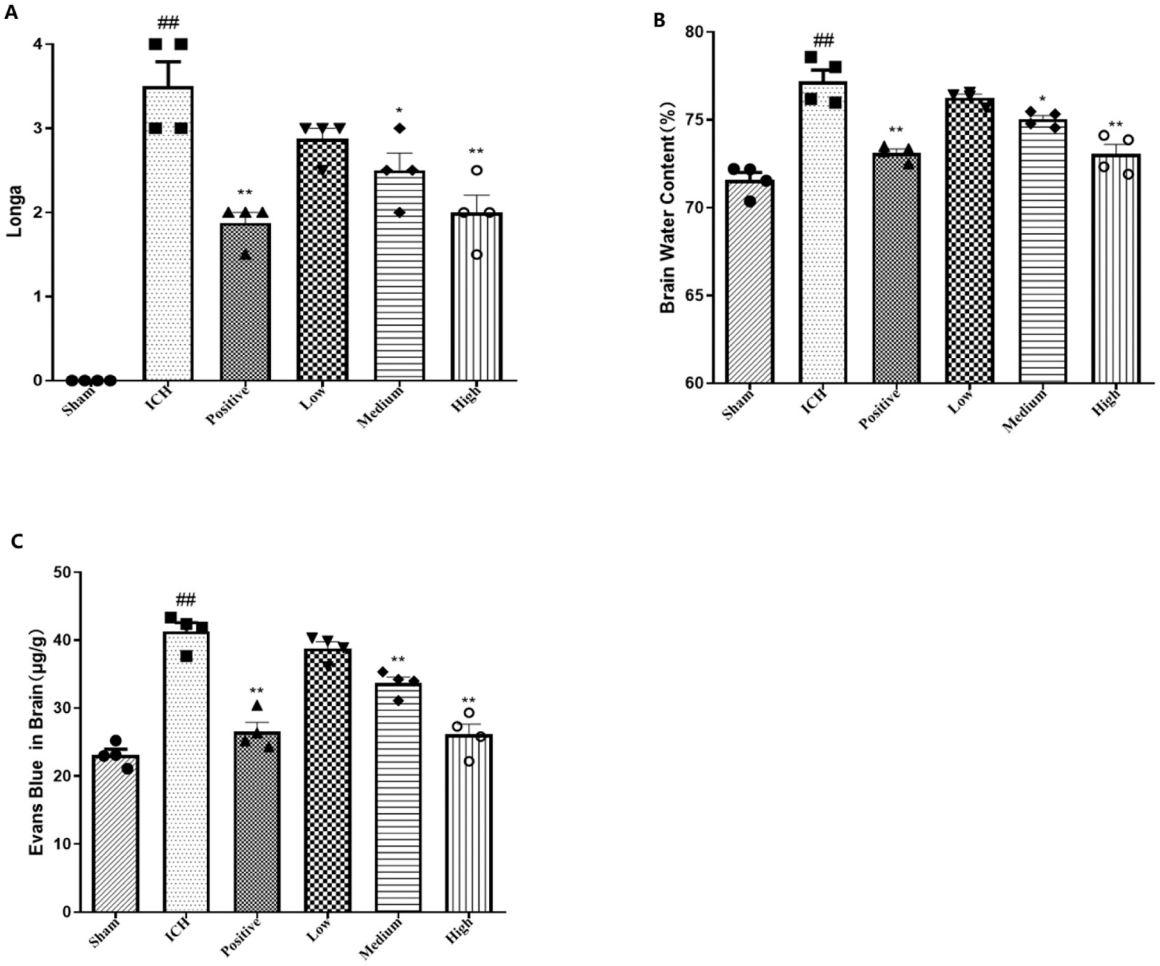

Fig. 1. Celastrol ameliorated neurobehavioral deficits and blood-brain barrier disruption induced by ICH. (A) Longa score was used to assess the neurobehavioral impairment (n = 4/group). (B) Wet/dry method was used to measure the brain water content (n = 4/group). (C) Spectrophotometric determination of Evans Blue (EB) dye extravasation was used to assess the BBB damage (n = 4/group). ##p < 0.01 compared to Sham group; *p < 0.05, **p < 0.01 compared to ICH group. Low group is meaning ICH+Celastrol 1 mg/kg; Medium group is meaning ICH+Celastrol 2 mg/kg; High group is meaning ICH+Celastrol 4 mg/kg; Positive group is meaning ICH+Ferrostatin-1, 2 mg/kg.

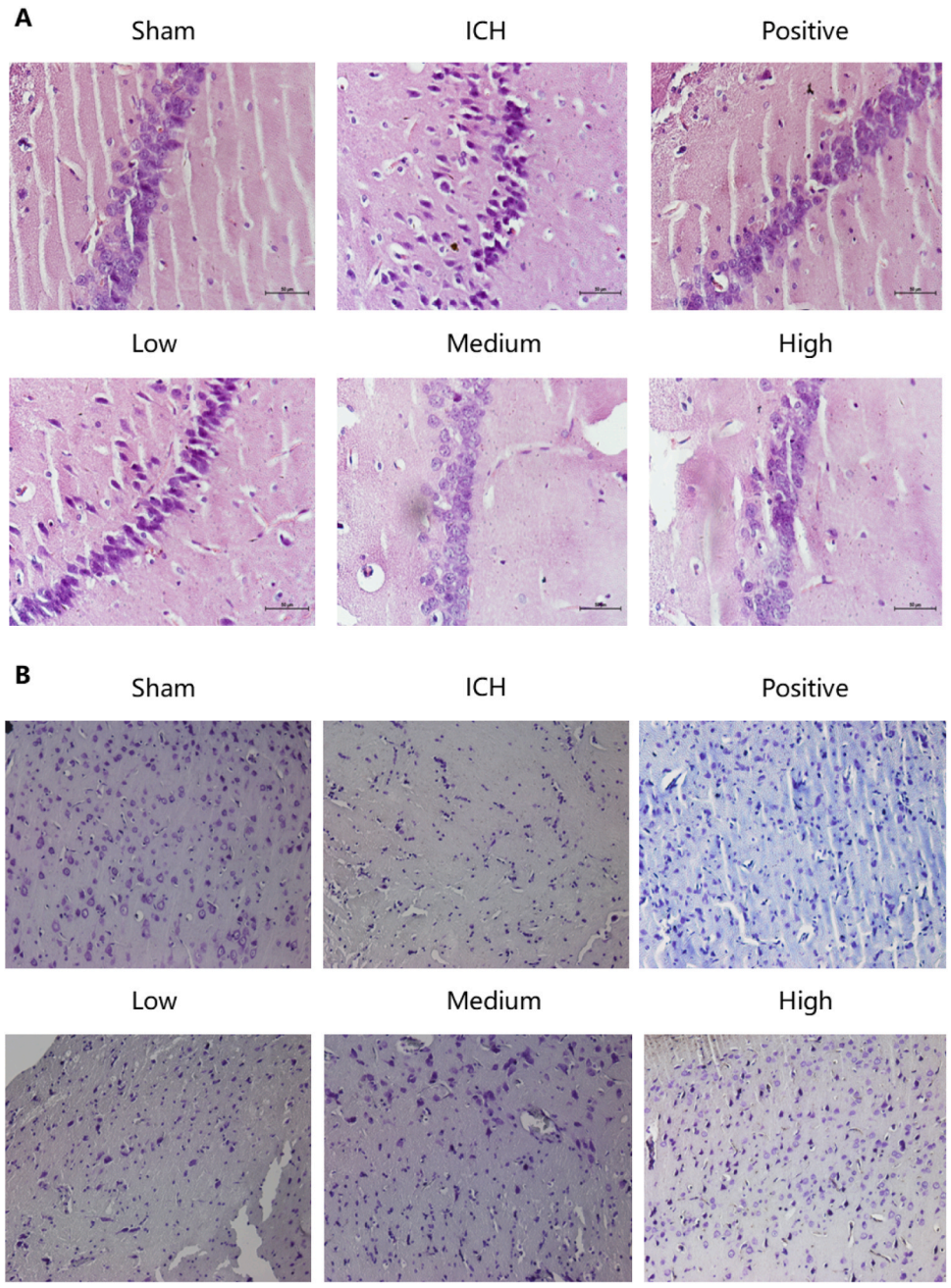

Fig. 2. Celastrol attenuated brain injury by ICH in a dose-dependent manner. (A) Morphological changes in the brain tissue were observed by HE staining after ICH injury. (B) Changes in Nissl staining after ICH injury were used to assess neuronal morphology.

antioxidative stress by reducing the production of reactive oxygen species (ROS) (Guan et al., 2016; Pan et al., 2019). Further, it prevents lipid peroxidation by exerting radical-scavenging properties. Celastrol inhibits peroxidation of the outer and inner mitochondrial membranes via radical scavenging, preventing oxygen radical assault on the inner membrane. This mechanism enhances the negative charge on the mitochondrial surface, offering an additional defence against oxidative free radicals(Zhang et al., 2017). Moreover, Celastrol can cross the blood-brain barrier, where it exerts protective effects against Parkinson's disease and Alzheimer's disease(Lin et al., 2019; Zhang et al., 2021b; Chow et al., 2014). Together, these studies suggest that celastrol could exert beneficial effects against subarachnoid haemorrhage and cerebral ischemia/reperfusion injury(Xu et al., 2021; Chen et al., 2022). However, research on celastrol in ICH is limited, and its effects and molecular mechanisms are not yet fully understood.

In this study, we examined the protective role of celastrol in an oxy hemoglobin (OxyHb)-induced injury model using PC12 cells and ICH model rats to elucidate its potential mechanism of action and binding sites.

2. Materials and methods

2.1. Materials

Reagents/materials were as follows: PC12 cells (Cat No.CL0412, Procell, China), Celastrol (Cat No.C408328, aladdin, China), ACSL4 (Cat No.ab155282, Abcam, UK), GPX4 (Cat No.ab125066, Abcam, UK), FTH1 (Cat No.ab183781, Abcam, UK), TFR1 (Cat No.ab269513, Abcam, UK),RIPA lysis buffer (Cat No. C0481, Sigma–Aldrich), BCA kit (Cat No. 23227, Thermo Fisher Scientific), Fe2+, ROS, MDA, SOD, CAT, and GSH

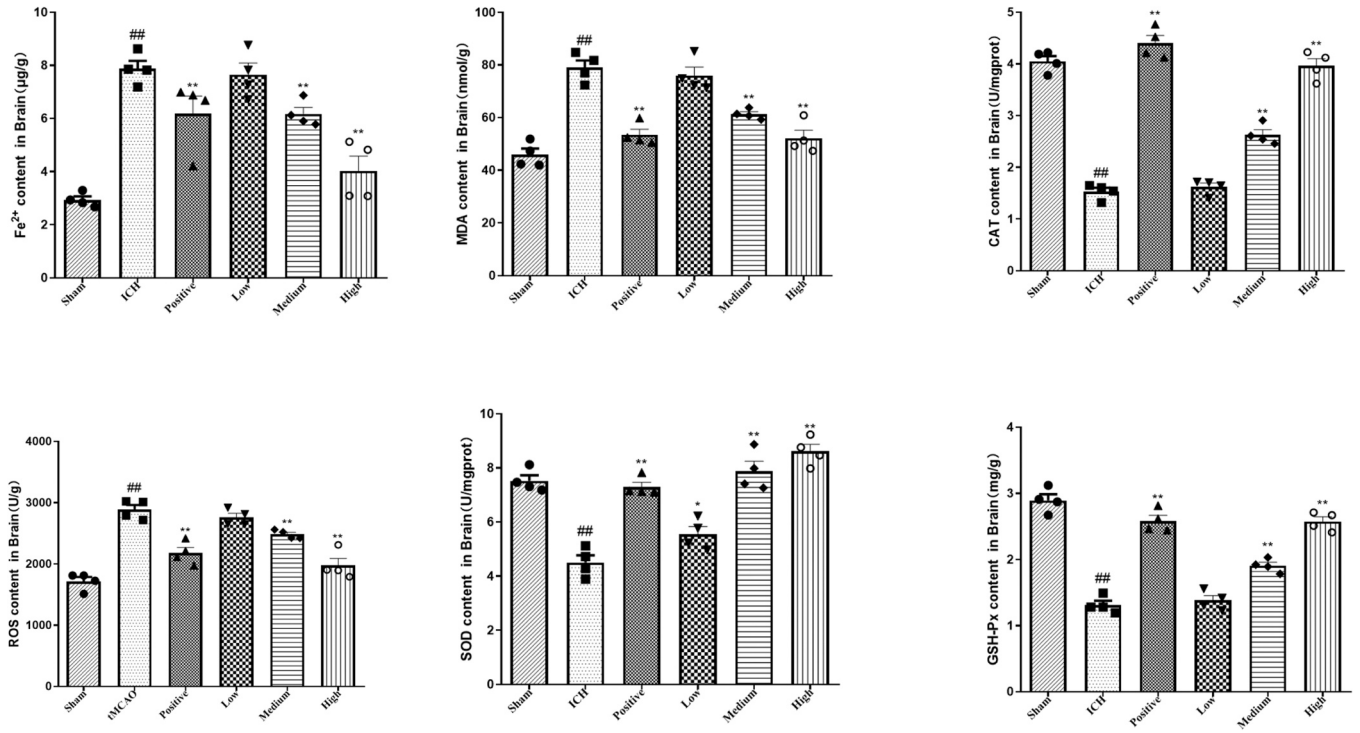

Fig. 3. Detection of cortical Fe2+, ROS, MDA, SOD, CAT and GSH-Px levels was using relevant commercial kits.(n = 4/group). ##p < 0.01 compared to Sham group; *p < 0.05, **p < 0.01 compared to ICH group. Low group is meaning ICH+Celastrol 1 mg/kg; Medium group is meaning ICH+Celastrol 2 mg/kg; High group is meaning ICH+Celastrol 4 mg/kg; Positive group is meaning ICH+Ferrostatin-1, 2 mg/kg.

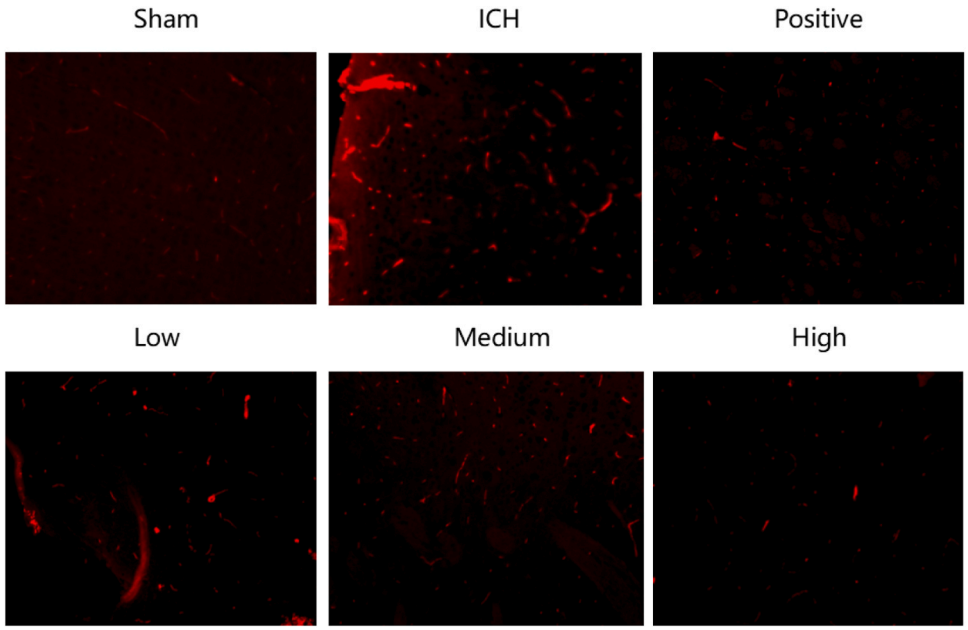

Fig. 4. Labelling of ROS in cortical sections was using the fluorescent probe dihydroethidium. Low group is meaning ICH+Celastrol 1 mg/kg; Medium group is meaning ICH+Celastrol 2 mg/kg; High group is meaning ICH+Celastrol 4 mg/kg; Positive group is meaning ICH+Ferrostatin-1, 2 mg/kg.

(Cat No. A039–2–1、E004–1–1、A003–1–2、A001–3、A007–1–1、A006–1–1, Jiancheng, Nanjing, China), Ferrostatin-1 (Cat No. HY-100579, MedChemExpress, US), TRIzol™Plus RNA kit (Cat No. 12183555, Thermo Fisher, US), Goat anti-rabbit IgG (Cat No. PV6000, Jinqiao, China)

2.2. Animals and experimental groups

Male Sprague–Dawley rats (n = 42), aged 6–8 weeks, and weighing 220 ± 20 g, were purchased from Yangzhou University. All animal experiments were approved by the Animal Experiment Ethics Committee of the Yangzhou School of Clinical Medicine of Dalian Medical University. The rats were housed under suitable temperature and humidity conditions, and provided with access to food and water ad libitum.

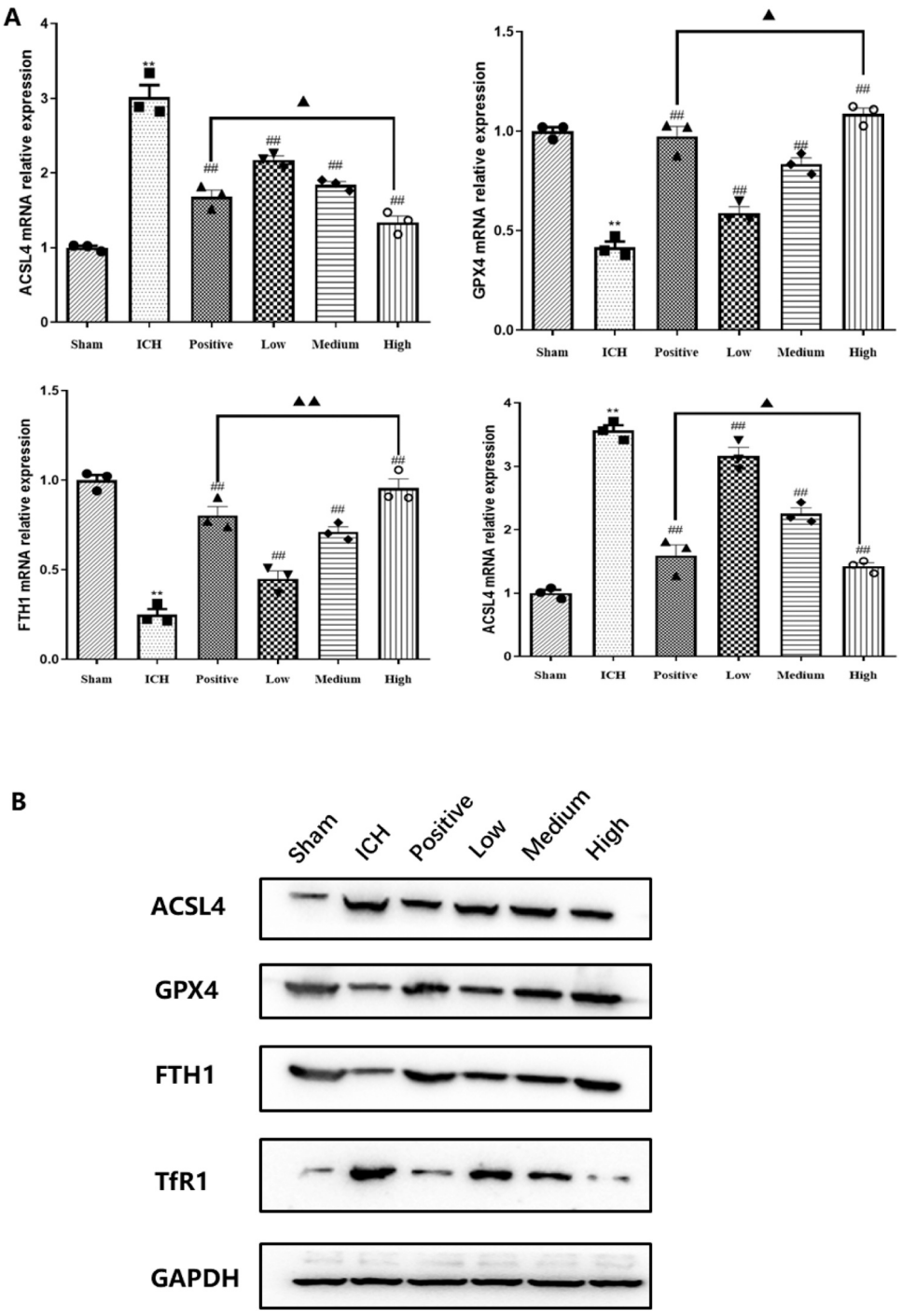

Fig. 5. Celastrol attenuated ICH-induced neuronal cell ferroptosis. (A) Expression of ferroptosis-related factors was detected by qPCR. (B) Western blot was used to detect the ferroptosis-related protein expression levels. **p < 0.01 compared to Sham group. ##p < 0.01 compared to ICH group; ▲p < 0.05, ▲▲p < 0.01 compared to Positive group. Low group is meaning ICH+Celastrol 1 mg/kg; Medium group is meaning ICH+Celastrol 2 mg/kg; High group is meaning ICH+Celastrol 4 mg/kg; Positive group is meaning ICH+Ferrostatin-1, 2 mg/kg.

Following a one-week acclimatization period, the rats were allocated into six groups, each comprising seven rats (with a minimum of six rats per group to mitigate the risk of mortality): sham group, ICH group, ICH+Celastrol low dose group (1 mg/kg), ICH+Celastrol medium dose group (2 mg/kg), ICH+Celastrol high dose group (4 mg/kg), and ICH+positive drug group (Ferrostatin-1, 2 mg/kg).

The ICH model was prepared by the stereotactic injection of collagenase VII (250 U/ml) into the right basal ganglia region(Jia et al., 2020). Using the bregma as the reference point, a small bone flap approximately 1 mm in diameter was drilled in the surgical positioning area, defined as 0.2 mm posterior to bregma and 3.0 mm right lateral to the midline. Either saline or 2 μl collagenase VII was infused at a depth of 6 mm, at a rate of 0.4 μl/min using a microinjection pump. The needle was then removed after 10 min. Finally, the bone hole was sealed with bone wax, and the incision was sutured and disinfected. Finally, rats were placed in separate cages with ad libitum access to food and water. The rats were treated with either 0.9 % NaCl solution (Sham group and ICH group), corresponding doses of celastrol (the equivalent to the clinical dose), or Ferrostatin-1 at a dose of 2.5μmol/kg via intraperitoneal injection (positive drug group) over a 7d period, once per day. The

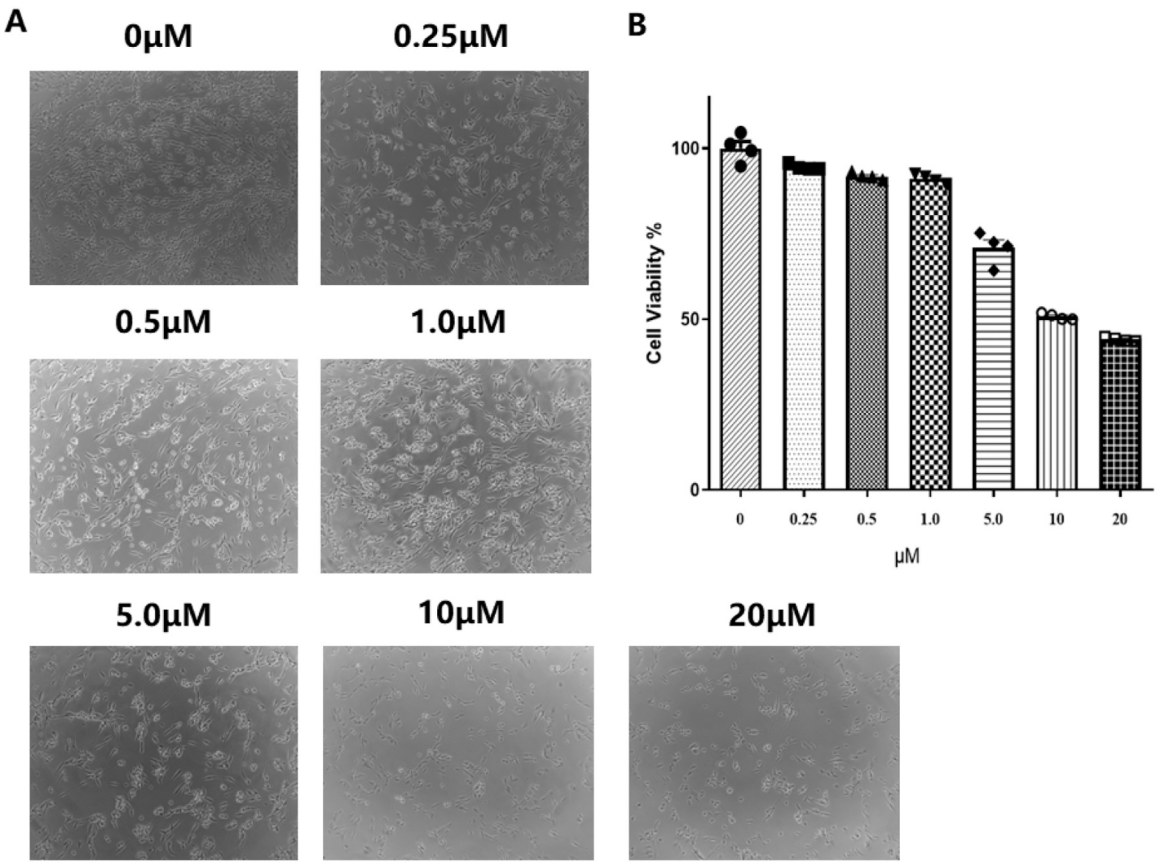

Fig. 6. Celastrol treatment inhibited the viability of PC12 cells by the MTT assay. (A) Effect of different doses of celastrol on morphology of PC12 cells was visualized with the microscope. (B) Effect of different doses of celastrol on activity in PC12 cells was assessed.

ICH model was induced 1 h after drug administration, and subsequent experiments were conducted 24 h later.

2.3. Cell culture and cell transfection

PC12 cells were cultured in DMEM supplemented with 10 %FBS and 1 % penicillin/streptomycin, and incubated at 37°C in an atmosphere of 5 % CO_2. The cells were then seeded in 96-well plates at a density of 5000 cells per well, and detached using 0.25 % trypsin-EDTA after reaching 90 % confluency for subculturing. The cells were subjected to various tests and analyses after passaging for three generations. Finally, an in vitro ICH model was established involving subjection of the neurones to stimulation with OxyHb (20 μl) at 37 ℃ with 5 % CO_2 for 6 h for subsequent experiments. The hippocampal neurones were assigned in one of the following groups: control group (neurones without any treatment); OxyHb group (neurones exposed to 20 μM OxyHb for 24 h); OxyHb+celastrol low dose group (0.25 μM); OxyHb+Celastrol medium dose group (0.5 μM); and OxyHb+Celastrol high dose group (1 μM).

The ACSL4 overexpression vector and its respective negative control were procured from GenePharma (Shanghai, China). PC12 cells were transfected at a 20-fold multiplicity of infection (MOI), using Lipofectamine 3000 (Invitrogen). At 48 hours after transfection, the cells were subjected to puromycin selection. The efficiency of overexpression was assessed by western blot analysis.

2.4. Neurological function scores in rats

Neurological function was assessed using the Longa scale for 24 h, with scoring performed as follows: 1. No neurological deficit: 0 points, 2. Inability to fully extend the front paw on the paralysed side: 1 point, 3. Turning to the paralysed side while walking: 2 points, 4. Leaning toward the paralysed side while walking: 3 points; 5. Inability to walk automatically and loss of consciousness: 4 points.

2.5. Evans blue extravasation assay

To evaluate changes in blood-brain barrier permeability, Evans blue dye was used as an indicator of albumin extravasation. Rats received an intravenous injection of 2 % Evans Blue dye. Following 2 h of circulation, phosphate-buffered saline was perfused through the cardiac vein, and the brain tissue was extracted, homogenised, and centrifuged. The resulting supernatant was collected and spectrophotometrically measured at 620 nm.

2.6. Brain water content detection

Wet and dry weight methods were used to assess the water content of brain tissue in each group of rats. Following anaesthesia, the rat heads were decapitated, and their brains were removed. The cerebellum and lower brainstem were excised and weighed to determine wet brain weight. Subsequently, the brain was baked at 110°C for 48 hours to obtain the dry weight. From these measurements, the brain water content was calculated using the formula: brain water content (%) = (brain wet weight - brain dry weight) / brain wet weight × 100 %.

2.7. HE staining and Nissl staining

Haematoxylin and eosin (HE) staining was performed as follows: Brain tissue sections, 5μm thick, were stained with haematoxylin for 1 min, rinsed three times with double-distilled water, incubated with acidic ethanol for 30 seconds, immersed in eosin for 50 seconds, dehydrated in gradient ethanol, cleared in xylene, and cover slipped with

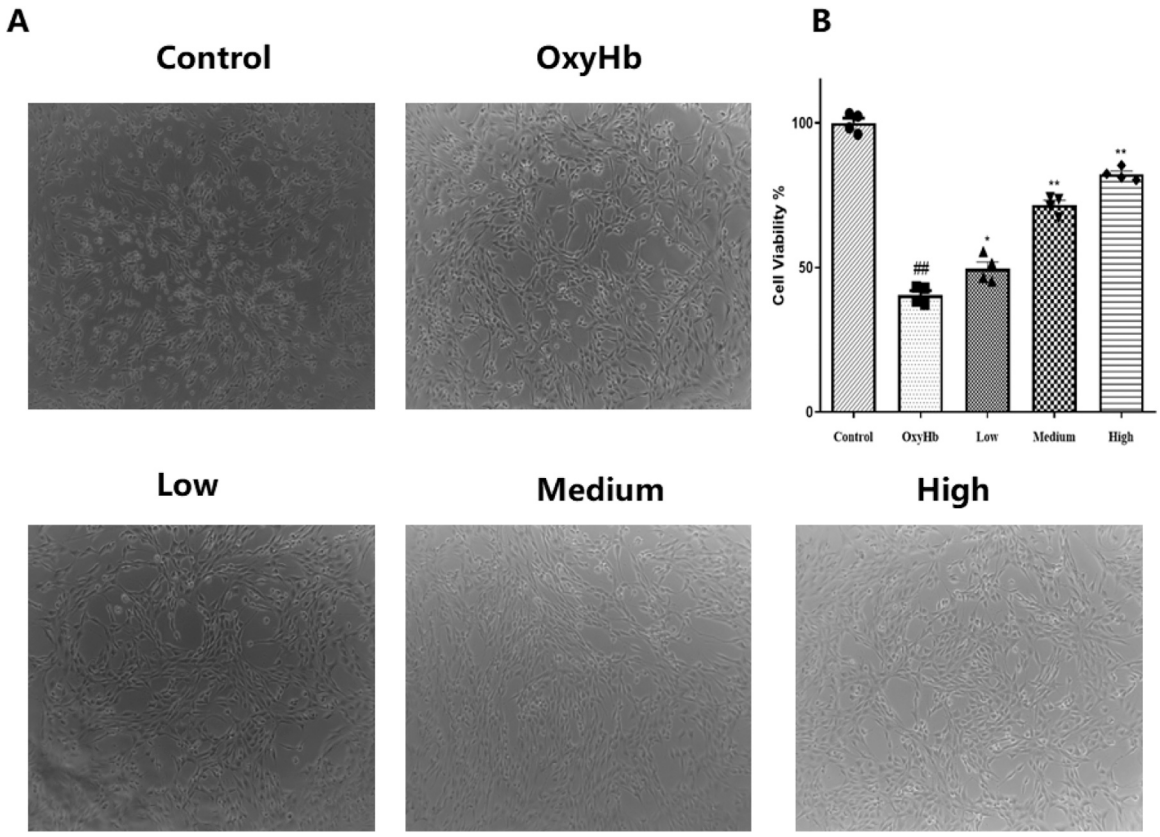

Fig. 7. Effect of celastrol on the viability of PC12 cells induced by OxyHb. (A) Effect of different doses of celastrol on morphology of OxyHb-exposed PC12 cells was visualized with the microscope. (B) Effect of different doses of celastrol on the viability of OxyHb-exposed PC12 cells was assessed.

neutral resin. Finally, the sections were observed under a microscope.

The brain tissue, 5μm thick, was immersed in 0.1 % cresyl violet for 6 minutes, followed by washing with double-distilled water. After dehydration in an alcohol gradient and dewaxing in xylene, the mixture was covered with neutral resin. Finally, the changes in the Nissl bodies were observed under a microscope.

2.8. qPCR detection of ferroptosis-related factor expression

Total RNA was extracted using the TRIzol kit (Invitrogen; Thermo Fisher Scientific, Inc.), followed by reverse transcription using a reverse transcription kit (Takara Biotechnology Co., Ltd., Dalian, China). PCR amplification of ACSL4, GPX4, FTH1, and TFR1 was performed using a PCR instrument to determine their mRNA expression levels. The mRNA level of GAPDH served as an internal control for normalization. The primer sequences were showed in the Table 1. The $2^{-\triangle\triangle Ct}$ method was used to present the multiple relationship between the target gene expression of the experimental group and the control group.Table 1

2.9. Western blot analysis

Total proteins were extracted from tissues or cells using high-efficiency RIPA buffer, in strict accordance with the manufacturer's instructions. The protein concentration of each sample was subsequently determined using a BCA kit. The proteins were then separated by sodium dodecyl sulphate–polyacrylamide gel electrophoresis (SDS-PAGE) and transferred to a polyvinylidene fluoride (PVDF) membrane. The membranes were then blocked with TBST buffer at room temperature for 1 h. Membranes were incubated overnight with primary rabbit antibodies against ACSL4 (1:1000), GPX4 (1:1000), FTH1 (1:1000), TFR1 (1:1000), and glyceraldehyde-3-phosphatedehydrogenase (GAPDH) (1:5000). On the second day, the membrane was washed with TBST and incubated with secondary antibodies at room temperature for 1.5 h. After incubation, the membranes were subjected to enhanced chemiluminescence quantification. Quantitative protein analysis was conducted using ImageJ 1.48 u software (Bio-Rad, Hercules, CA, USA). Relative protein levels were determined using the ratio of the grey value of each protein to that of the internal reference, GAPDH. Proteins were extracted and quantified, followed by the addition of primary antibodies (ACSL4, GPX4, FTH1, TFR1, and GAPDH antibodies) and secondary antibodies according to established protocols. The target protein bands were visualised using a chemiluminescence imager, and images were quantitatively analysed.

2.10. MTT screening for safe concentration of celastrol

PC12 cells in the logarithmic growth phase were adjusted to a concentration of 5×10^4 cells/ml, and seeded into a 96-well plate at 100 μl per well, with four replicate wells for each group. The outer wells were filled with 0.01 mol/l sterile PBS to prevent edge effects, and the cells were cultured at 37℃ with 5 % CO_2. After 24 hours, the culture medium was removed, and 100 μl of different concentrations (0, 0.25, 0.5, 1.0, 5.0, 10, 20 μM) of drug-containing medium was added to the wells. After 48 h, the culture supernatant was carefully removed, and 5 mg/ml MTT was added and incubated for 4 h. Subsequently, 150 μl of DMSO was added and incubated for an additional 10 minutes. The absorbance was finally measured at 490 nm using a microplate reader.

The experimental groups included the Control group, OxyHb group, OxyHb+Celastrol low dose group (0.25 μM), OxyHb+Celastrol medium dose group (0.5 μM), and OxyHb+Celastrol high dose group (1 μM). The pretreated cells were exposed to 5 mg/ml MTT for 4 hours, followed by the addition of 150 μl DMSO and further incubation for 10 minutes. Absorbance was measured at 490 nm using a microplate reader. The cell morphology was observed and photographed under an inverted

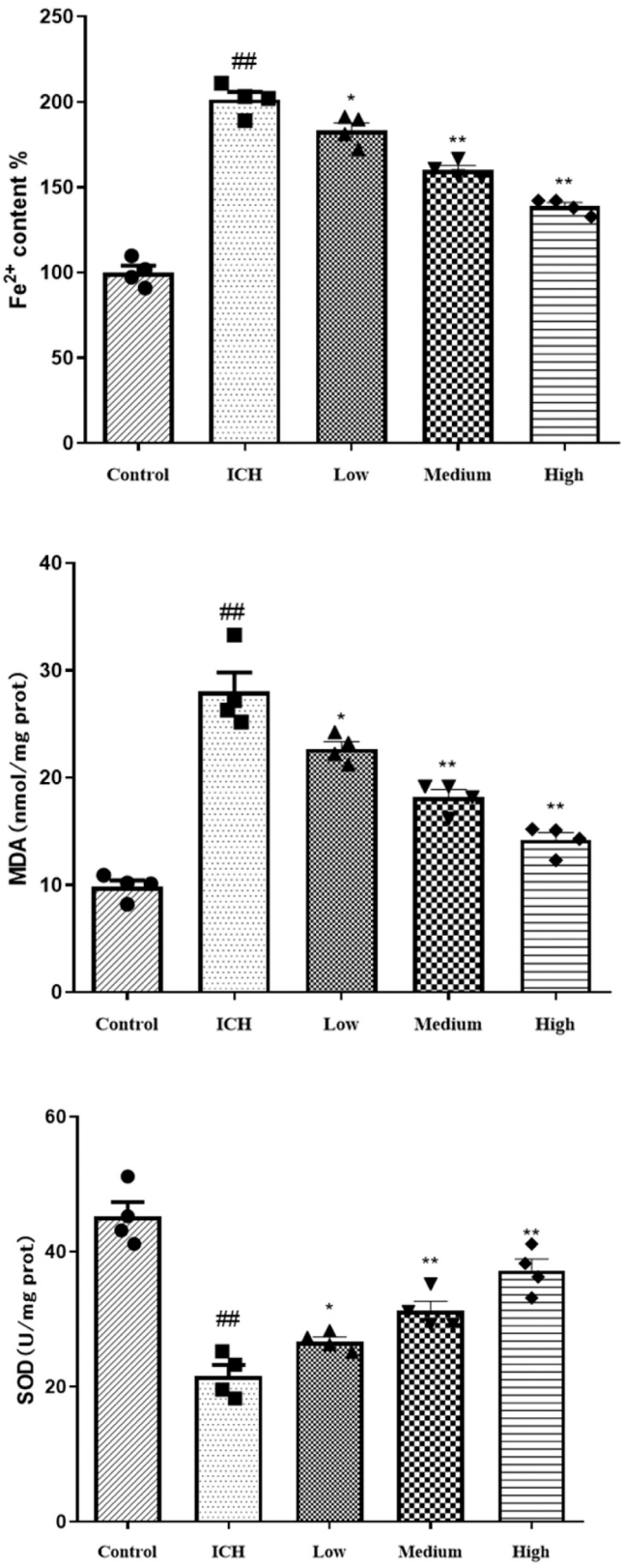

Fig. 8. Detection of cellular Fe2+, MDA, and SOD levels was using the corresponding commercial kits. ##p < 0.01 compared to Control group; *p < 0.05, **p < 0.01 compared to ICH group. Low group is meaning ICH+Celastrol 1 mg/kg; Medium group is meaning ICH+Celastrol 2 mg/kg; High group is meaning ICH+Celastrol 4 mg/kg.

microscope in a randomly-selected field of view.

2.11. Immunofluorescence

To assess ROS levels in vitro, cells were rinsed with PBS, and subsequently treated with 2′,7′-dichlorodihydrofluorescein diacetate (DCF; diluted 1:1000 in serum-free medium) for 30 min. Hoechst stain (diluted 1:2000 in serum-free medium) was added and incubated for 10 min. The cells were then rinsed with serum-free medium and examined under a fluorescence microscope.

2.12. Flow cytometry assay

Cells in the logarithmic phase were suspended and resuspended at a concentration of 1×10^6cells/ml. Subsequently, 100 μl of cell suspension was transferred into a flow tube and labelled with 10 μl of fluorescently labelled rabbit anti-rat antibody against ROS. Following a 30-minute incubation at 4°C in a light-protected refrigerator, the unbound antibody was removed by washing with PBS, and the samples were then analysed using flow cytometry.

2.13. Statistical analysis

All data were analysed by the software SPSS 26.0, and results were expressed as the mean ± standard deviation. Statistical analysis between two groups was performed using the Student's t-test, while multiple group comparisons were performed using ANOVA. Statistical significance was set at $p < 0.05$. difference.

3. Results

3.1. Celastrol protected blood-brain barrier and ICH injury in rats

The efficacy of celastrol in protecting the blood-brain barrier and motor impairment in the ICH model was evaluated using the Longa score, brain water content, and Evans Blue. In rats with intracerebral haematoma, the Longa score (Fig. 1A), brain water content (Fig. 1B), and Evans Blue extravasation around the brain tissue haematoma (Fig. 1C) were significantly higher than in the sham group. However, compared to the ICH group, these indices were significantly lower.

Under a pathological microscope (Fig. 2A), neuronal cells in the cerebral cortex of rats in the sham-operated group exhibited an orderly arrangement and normal structure. Conversely, the ICH model induced significant damage to the cortical area, resulting in the formation of numerous necrotic cells; this was evidenced by the disorganised brain tissue structure and the presence of crinkled and dense nuclei in neuronal cells. However, treatment with different concentrations of celastrol alleviated the ICH-induced abnormal changes in neuronal cells.

Nissl staining (Fig. 2B) revealed that the sham group had a high number of Nissl bodies in the hippocampal region, which were neatly arranged and deeply stained. In contrast, the ICH group showed a significant reduction in the number of Nissl bodies, along with a disordered arrangement and decreased staining intensity compared to the sham group. Following treatment with various concentrations of celastrol, we observed a notable increase in the number of Nissl bodies, accompanied by deeper staining and normalisation of the neuronal arrangement compared to the ICH group. These results strongly suggested that celastrol markedly ameliorated the blood-brain barrier and motor disability in the ICH model.

3.2. Celastrol suppressed ferroptosis in brain tissue of ICH rats

Rats with ICH were used to explore the possible role of celastrol in ICH injury. Compared to rats in the sham group, the ICH group exhibited markedly elevated levels of Fe2+, ROS, and MDA (Fig. 3), accompanied by increased red fluorescence intensity in the hippocampal neurones

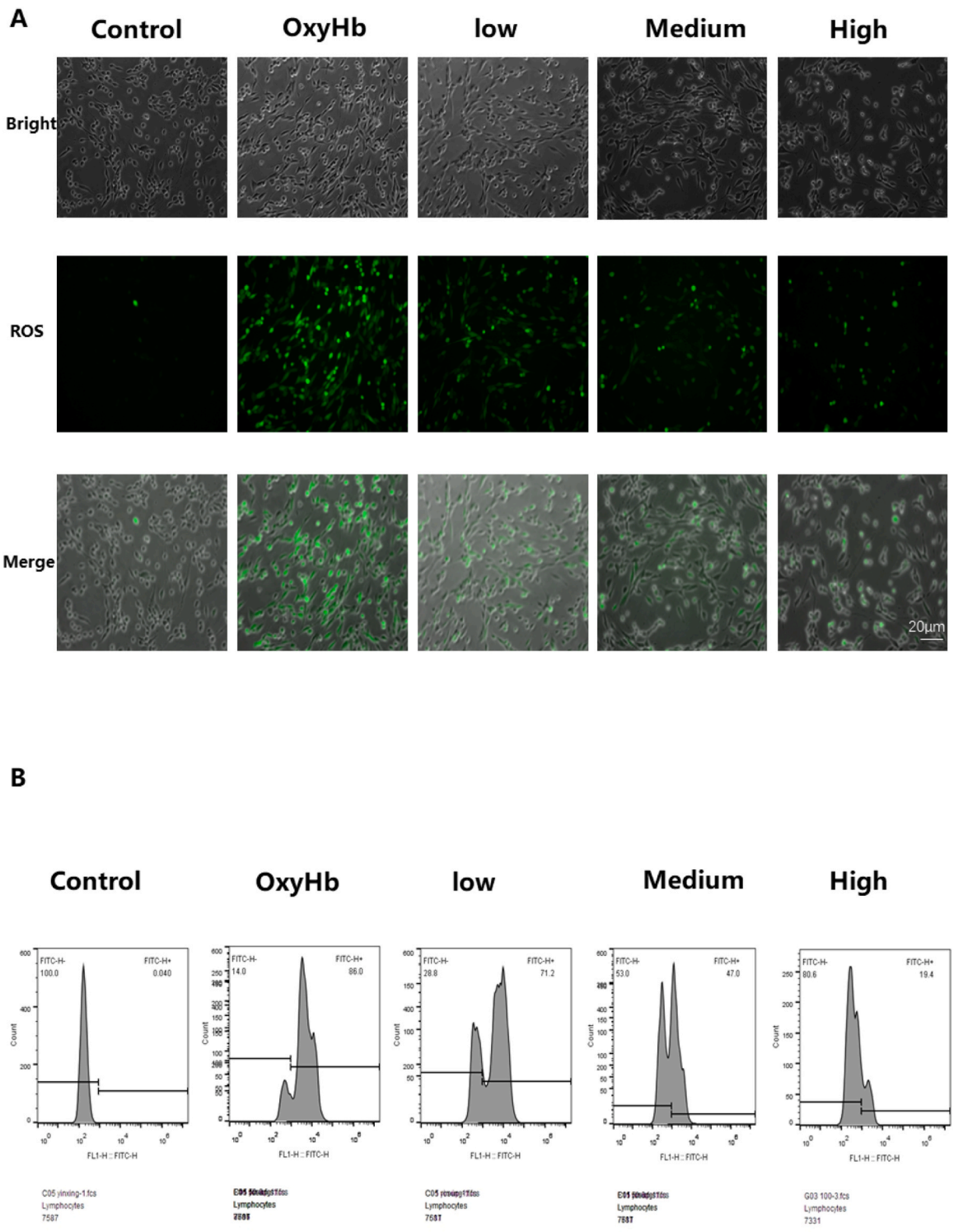

Fig. 9. Expression of ROS in PC12 cells treated with different concentrations of celastrol. (A) Immunofluorescence staining was used to detect the expression of reactive oxygen species (ROS), scale = 20 μm. (B) ROS expression was detected by flow cytometry in each group.

(Fig. 4), and increased mean fluorescence density. Conversely, the levels of SOD, CAT, and GSH-Px were significantly lower in the ICH group. Compared to the ICH group, rats treated with the positive drug (Ferristatin-1) and medium-to-high doses of celastrol demonstrated substantial reductions in Fe2+, ROS, and MDA levels, along with decreased ROS red fluorescence intensity and mean fluorescence density in hippocampal neurones. Moreover, SOD, CAT, and GSH-Px levels significantly increased.

The qPCR (Fig. 5A) and western blotting (Fig. 5 B) results clearly showed that ACSL4 and TFR1 levels were notably elevated, while GPX4 and FTH1 levels were significantly reduced in the ICH group compared to those in the sham group. Conversely, in comparison with the ICH group, the positive drug (Ferristatin-1) and various concentrations of celastrol intervention groups exhibited significantly lower ACSL4 and TFR1 levels, and higher GPX4 and FTH1 levels. Furthermore, the high-dose celastrol group demonstrated significantly lower ACSL4 and TFR1

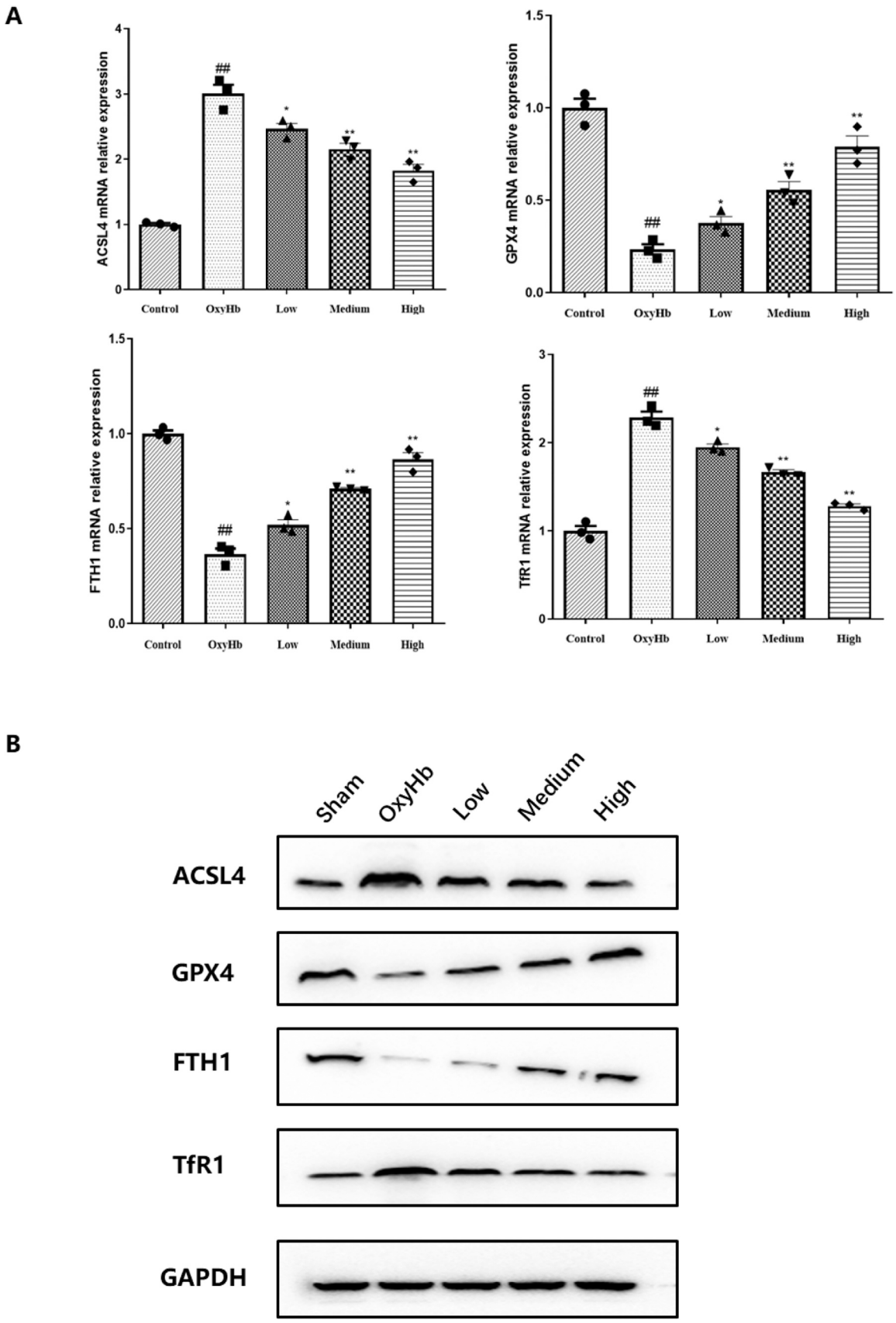

Fig. 10. Protein expressions of Acsl4, GPX4, FTH1 and TFR1 in PC12 cells treated with different concentrations of celastrol. (A) qPCR assessing was used to detect the expression of ferroptosis-related factors. (B) Western blot was used to detect the expression levels of ferroptosis-related proteins. ##$p < 0.01$, compared to Control group; *$p < 0.05$, **$p < 0.01$, compared to OxyHb group.

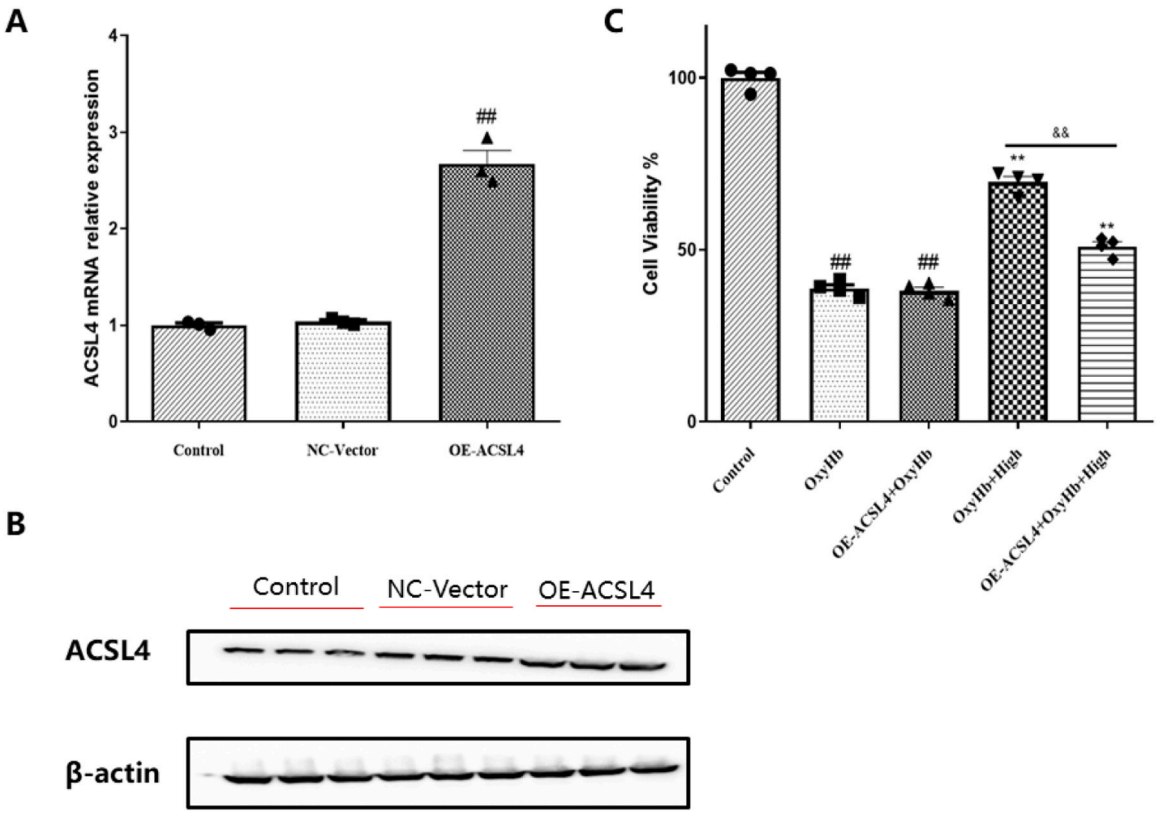

Fig. 11. Acsl4 was successfully overexpressed and transfected PC12 cells. (A) ACSL4 expression level was detected by qPCR. (B) Western blot assay was used to detect ACSL4 expression level. (C) MTT assay was used to detect cell viability. ##p < 0.01, compared with Control group; **p < 0.01, compared with OxyHb group; & & p < 0.01, compared with OxyHb+High group.

levels, and significantly higher GPX4 and FTH1 levels than the positive group (Ferristatin-1).

3.3. Celastrol exerted a protective effect on neuronal cells by inhibiting ferroptosis

3.3.1. Dose response: 1.0 μM celastrol could safely retain cell activity

In vitro experiments were conducted using OxyHb to observe the effects of celastrol on ICH cells. On the MTT assay (Fig. 6 A.B), the number of cells exhibiting wrinkled, rounded, and clustered growth decreased following treatment with various concentrations of celastrol under normal culture conditions. Notably, even at a drug concentration of 1.0 μM, over 90 % of cell activity was retained; as such, this concentration was chosen for subsequent experiments.

3.3.2. Celastrol protected neurons in a dose-dependent manner on ICH injury

In the Control group, cell growth appeared more robust (Fig. 7A), with a greater abundance of cells exhibiting a flatter and elongated morphology. Conversely, the ICH group displayed a lower cell count, with an increased presence of dead cells and cellular debris. Compared with the model group, we observed a notable augmentation in the viable cell count and normalisation of cell morphology in the celastrol low-, medium-, and high-dose treatment groups. Treatment with low, medium, and high doses of celastrol (Fig. 7B) led to an increase in the viable cell count compared to that in the OxyHb group. Therefore, the results showed that celastrol may protect neuronal cells from ICH injury in a dose-dependent manner.

3.3.3. Celastrol ameliorated ICH injury by suppressing ferroptosis in vitro

In vitro experiments further showed that celastrol suppressed the release of oxidative stress factors and inhibited the expression of ferroptosis-related proteins. Compared with the Control group (Fig. 8), Fe2+ and MDA levels were significantly higher, while SOD levels were significantly lower in the OxyHb group. Compared to the OxyHb group, Fe2+ and MDA levels were significantly lower, and SOD levels were significantly higher in the low-, medium-, and high-dose celastrol treatment groups.

Compared with the Control group (Fig. 9A), the ROS green fluorescence intensity was enhanced, while the mean fluorescence density was increased in the OxyHb group; compared with the OxyHb group, the ROS green fluorescence intensity was reduced and the mean fluorescence density was decreased in the celastrol low, medium and high dose treatment groups. Celastrol reduced intracellular ROS levels (Fig. 9B).

3.4. Celastrol inhibited ferroptosis after neuronal injury via the ACSL4 pathway

Based on the above results, we suspected that celastrol could inhibit ferroptosis after neuronal injury via the ACSL4 pathway. To asses this, the relative mRNA expression levels of ACSL4, GPX4, FTH1, and TFR1 were detected using qPCR (Fig. 10A) and western blotting (Fig. 10 B). The ACSL4 and TFR1 levels were significantly higher in the OxyHb group than in the control group. Additionally, GPX4 and FTH1 levels were significantly decreased in the OxyHb group. However, celastrol altered the expression of ferroptotic proteins.

ACSL4 played an important role in ferroptosis qPCR (Fig. 11A), while western blotting (Fig. 11B) showed that the cells were significantly transfected with ACSL4, indicating successful ACSL4 overexpression. Cell viability was significantly reduced by OxyHb compared to controls (Fig. 11C). Cell viability was significantly lower in the OE-ACSL4+OxyHb+High group than in the OxyHb+High group. The results showed that cell viability increased in the celastrol group. In contrast, ACSL4 overexpression had the opposite effect. Compared to the

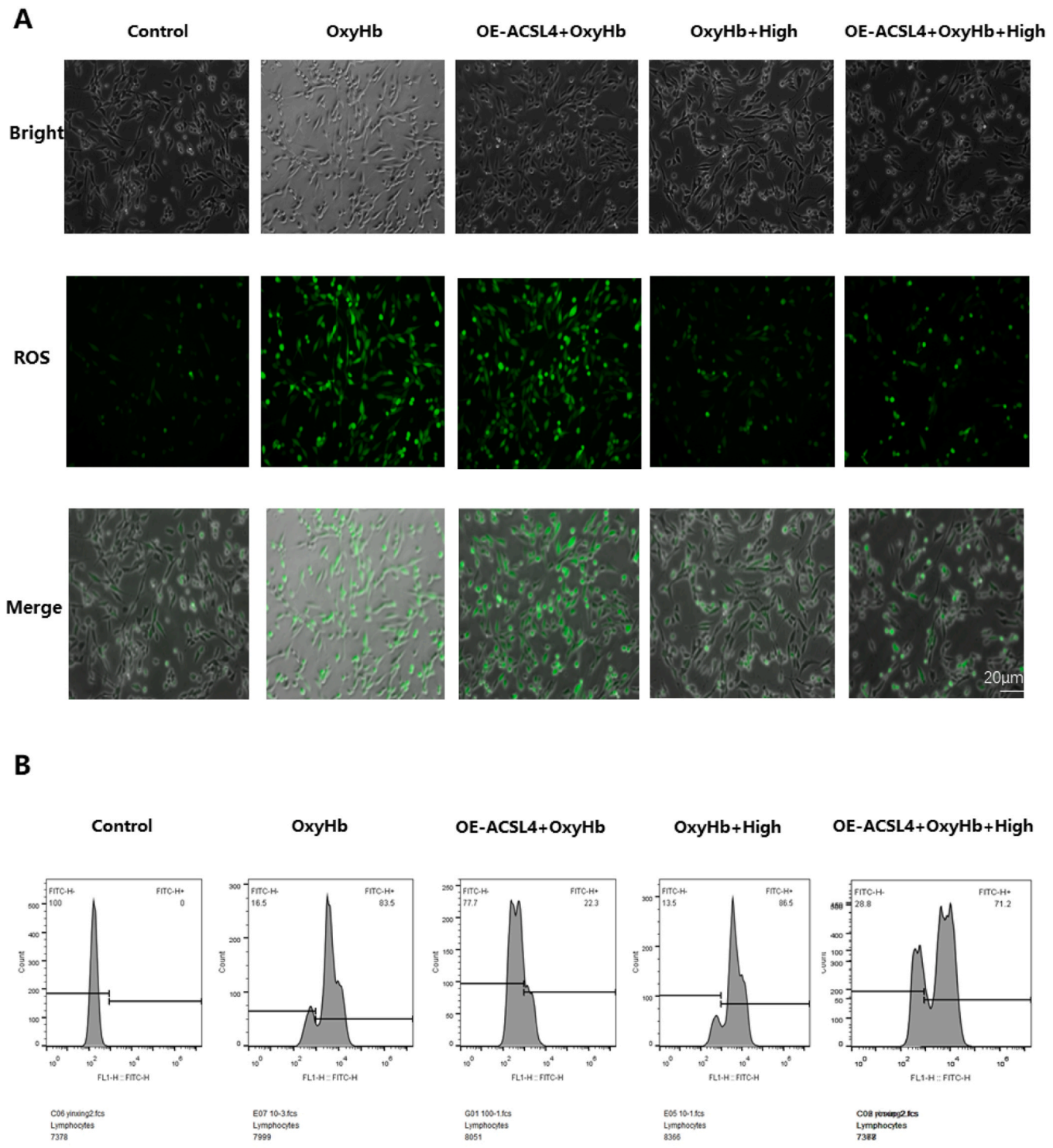

Fig. 12. Celastrol and Acsl4 co-treatment reduced expression of ROS in PC12 cells induced by OxyHb. (A) Immunofluorescence staining was used to detect ROS expression, scale = 20μm. (B) Flow cytometry was used to detect cellular ROS expression level in each group.

control group, ROS fluorescence intensity (Fig. 12A) was enhanced, and the mean fluorescence density increased in the OxyHb group. Besides, the overexpression of ACSL4 regulated ROS production. Similar results were observed with flow cytometry (Fig. 12B).

In vivo experiments further showed that celastrol suppressed the release of oxidative stress factors and inhibited the expression of pro-ferroptosis-related proteins. Compared with the Control group (Fig. 13), Fe2+ and MDA levels were significantly higher and SOD levels were significantly lower in the OxyHb group. Fe2+ and MDA levels were also significantly higher and SOD levels were significantly lower in the OE-ACSL4+OxyHb+High group compared to the OxyHb+High group. As the results demonstrated (Fig. 14 A.B), compared with the Control group, the levels of ACSL4 and TFR1 were significantly higher in the OxyHb group, while the levels of GPX4 and FTH1 were significantly lower. Compared with the OxyHb group, the OxyHb+High and OE-ACSL4+OxyHb+High groups ACSL4 and TFR1 levels were significantly higher. Finally, ACSL4 and TFR1 levels were significantly lower in the OE-ACSL4+OGD/R+High group than in the OxyHb+High group.

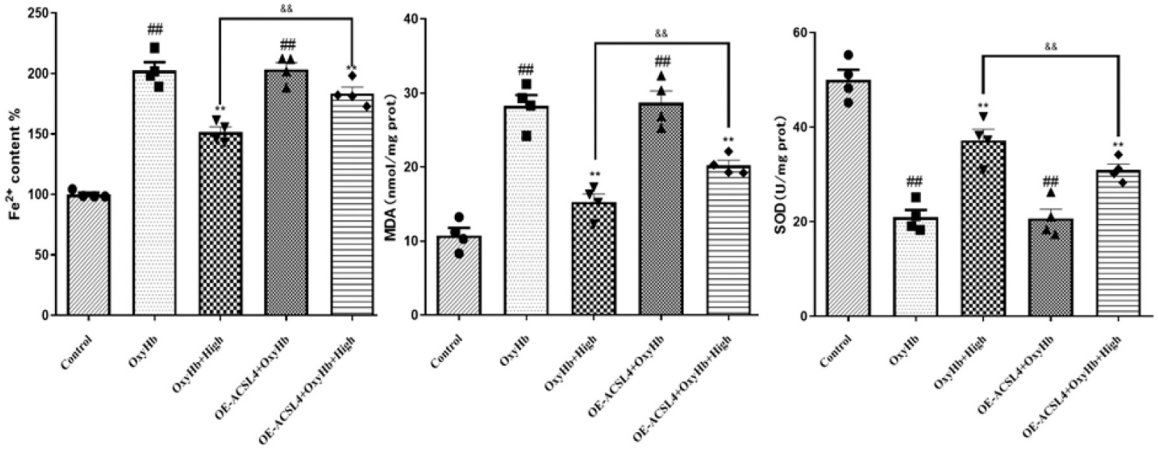

Fig. 13. Detection of cellular Fe2+, MDA, and SOD levels was using the corresponding commercial kits. ##p < 0.01, compared with Control group; **p < 0.01, compared with OxyHb group; & & p < 0.01, compared with OxyHb+High group.

3.5. Molecular docking analysis of the binding sites of herbal monomers to ACSL4

Molecular docking analysis was performed using AutoDock (Fig. 15) to explore the potential mechanism of celastrol regulation by ACSL4. The results showed that celastrol bound to ACSL4 by forming stable hydrogen bonds at the GLU107, GLN109, ASN111, and LYS357 sites.

4. Discussion

ICH is the most severe stroke complication. ICH can cause primary and secondary brain damage during the pathological response(Bonsack et al., 2017; Leclerc et al., 2018), is associated with damage and subsequent neurological dysfunction resulting from the restoration of blood flow to the brain tissue following a transient period of haemorrhage. Primary cerebral damage is caused by the physical disruption of the cellular architecture. Moreover, haematoma can cause oxidative damage, inflammation, glutamate toxicity, blood–brain barrier disruption, and neuronal death, leading to secondary damage to the brain tissue(Wu et al., 2013; Zhu et al., 2015; Yang et al., 2018; Qu et al., 2019). The pathophysiological mechanisms underlying ICH are highly intricate, involving the interplay between various cellular death pathways and molecules. These include neuronal injury, oxidative stress, inflammatory response, neuronal apoptosis, ferroptosis, and autophagy. No treatment strategy to completely prevent or reverse the onset and progression of ICH has yet been identified. Hence, finding new ways to minimise the damage to brain cells caused by haematomas is a crucial focus of stroke treatment research.

Celastrol is a quinone methide triterpene isolated from Tripterygium wilfordii that has attracted considerable attention for more than 70 years for its potential medicinal properties(Zhang et al., 2017; Jiang et al., 2018). Celastrol exerts antioxidant effects through scavenging ROS(Guan et al., 2016). In the mitochondria, celastrol has been shown to have powerful antioxidant properties that prevent lipid peroxidation by scavenging radicals. Additionally, through an increase in the negative surface charge of mitochondria, celastrol can further protect the inner mitochondrial membrane from oxygen radical attack(Zhang et al., 2017), cross the blood–brain barrier, and exert therapeutic effects on neurological disorders such as Parkinson's disease and Alzheimer's disease(Chow et al., 2014; Lin et al., 2019; Zhang et al., 2017). In addition, celastrol exerts clear protective effects against subarachnoid haemorrhage and cerebral ischemia/reperfusion injury(Xu et al., 2021; Chen et al., 2022). Celastrol reduces the downregulation of tight junction proteins, such as occludin, claudin-5, and ZO-1, induced by oxygen-glucose deprivation, by activating the MAPKs and PI3K/Akt/mTOR pathways, thus maintaining the integrity of the blood-brain barrier (Luo et al., 2016). Early studies reported that celastrol could improve neurological function in a rat model of permanent middle cerebral artery occlusion, as well as reduce cerebral infarct volume, and that this neuroprotective effect was associated with the downregulation of ischaemic cortex p-JNK, p-c-Jun, and NF-κB expression by the drug(Li et al., 2012). However, the mechanism underlying the action of celastrol in ICH has not been fully elucidated.

Our study demonstrated that both moderate and high doses of celastrol notably enhanced neurological function in rats with ICH. Additionally, this drug inhibits blood-brain barrier disruption, thus alleviating brain oedema. Nissl bodies are organelles situated in neuronal cell bodies and dendrites that play pivotal roles in cell metabolism and protein synthesis. By examining the brain tissue in the hippocampal region of ICH rats, we observed that celastrol effectively mitigated ICH-induced hippocampal tissue damage. Moreover, intervention with various ICH concentrations notably increased the number of Nissl bodies in the hippocampal region. These findings demonstrated the role of celastrol in enhancing neuronal function recovery in the hippocampal regions of ICH rats.

Ferroptosis, a form of non-apoptotic cell death, causes iron-mediated oxidative damage. Excessive accumulation of ions triggers the generation of free radicals and oxidative stress, culminating increased lipid peroxidation, a crucial step in ferroptosis induction. Elevated intracellular Fe2+ levels lead to the production of ROS, resulting in increased levels of MDA, a byproduct of lipid peroxidation. This cascade accelerates oxidative stress, ultimately resulting in cell death. In ferroptosis, crucial functions are mediated by antioxidant enzymes, such as SOD, GSH-Px, and CAT. SOD protects cells from oxidative stress by converting harmful superoxide radicals into hydrogen peroxide and oxygen via a spontaneous disproportionation reaction(Fujii et al., 2022). GSH-Px and CAT decompose lipid peroxidation by-products and hydrogen peroxide into benign substances, thus exerting antioxidant effects(Liu et al., 2021). Recently, Tsvetkov (Tsvetkov et al., 2022) discovered a new form of cell death induced by copper ion carriers. The mechanism of cuproptosis might be linked to mitochondria, where the accumulation of copper ions in cells induces oligomerization of mitochondrial lipid acylated protein aggregates with reduced Fe-S cluster protein levels leading to proteotoxic stress(Qin et al., 2023). Cuproptosis could not be blocked by apoptosis inhibitors or ferroptosis(Zhao and Qi, 2023). In 2023, Liu(Liu et al., 2023) revealed that abnormal accumulation of disulfide occurs in SLC7A11-high cells under glucose starvation, which ultimately leads to disulfide stress and rapid cell death. Recent studies term this cell death disulfidptosis(Liu et al., 2023, Liu et al., 2020). The crosstalk between mitophagy and ferroptosis is an important contributor to some forms of cell death such as disulfidptosis. Selective autophagy mediated by nuclear receptor coactivator 4(NCOA4), which degrades

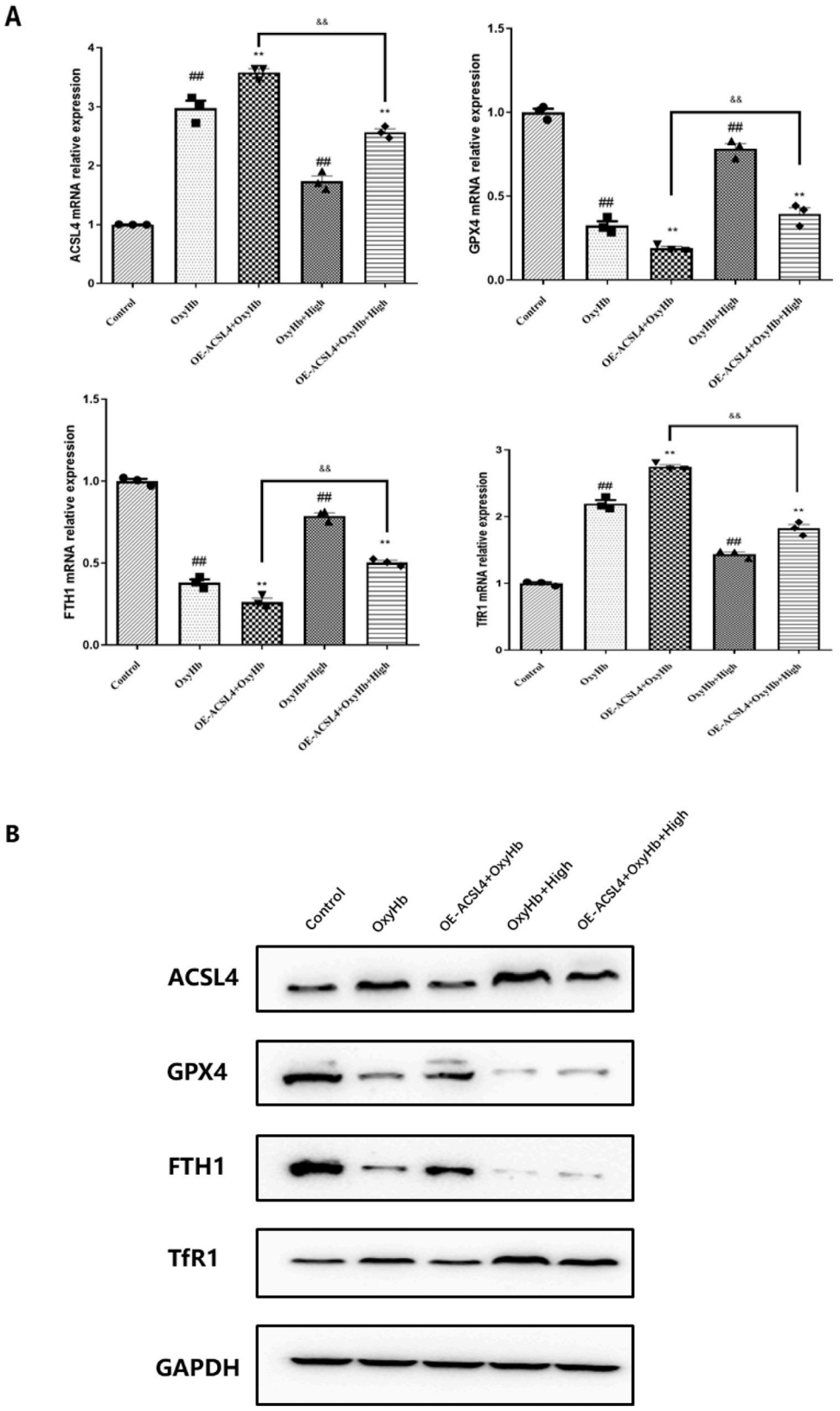

Fig. 14. Celastrol inhibited neuronal cells ferroptosis induced by ICH via Acsl4 overexpression. (A) qPCR was used to assess the expression of ferroptosis-related factors. (B) Western blot was used to detect the expression levels of ferroptosis-related proteins. ##p < 0.01, compared with Control group; **p < 0.01, compared with OxyHb group; & & p < 0.01, compared with OE-ACSL4+OxyHb group.

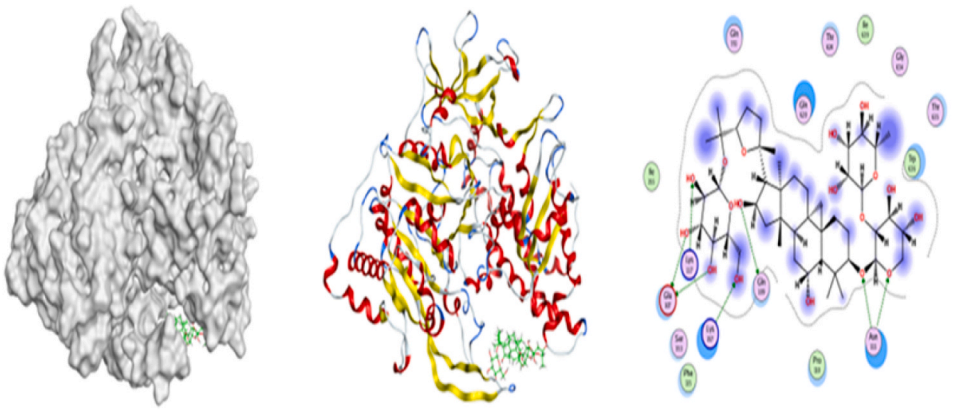

Fig. 15. Direct interactions between Celastrol and ACSL4 revealed by molecular docking. Docking score S = −8.118742 Kcal/mol; Number of interactions:7; Binding site: GLU107 / GLN109 / ASN111 / LYS357.

and releases free iron in autophagosomes(Su et al., 2024). Additionally, increased ferritin autophagy can lead to excessive intracellular iron accumulation and improve cell sensitivity to ferroptosis. Although cuproptosis and disulfidptosis associated with ICH had been identified, these findings mainly focus on bioinformatics analysis should be further investigated experimentally.

In the in vivo experiment, rats in the ICH group showed a marked increase in Fe2+ levels compared with those in the sham group, indicating an accumulation of iron ions due to haematoma injury. Additionally, we observed a notable increase in ROS and MDA levels, along with a decrease in SOD, CAT, and GSH-Px levels, indicating excessive generation of free radicals during cerebral haematoma. This results in lipid peroxidation reactions and a decrease in the antioxidant capacity of the body, leaving nerve cells vulnerable to oxidative damage. Following the administration of medium and high doses of celastrol, decreases in Fe2+, ROS, and MDA levels in ICH rats were observed. These results suggested that celastrol partially inhibited ferroptosis and oxygen free radical production during ferroptosis. Moreover, we observed a significant increase in SOD, CAT, and GSH-Px levels, indicating that celastrol effectively alleviated ICH-induced oxidative stress and protected the brain tissue from ferroptosis-related damage.

ACSL4 functions as a pivotal enzyme in lipid metabolism, and emerging research has indicated that it facilitates lipid peroxidation, thus triggering the liberation of iron ions and consequently inducing ferroptosis(Yang et al., 2022; Cui et al., 2021). Increased TFR1 expression is believed to contribute to cellular iron overload(Lan et al., 2023). In ferroptosis, GPX4 serves as a crucial antioxidant enzyme that catalyses the conversion of harmful substances, such as ROS and lipid peroxide, into relatively harmless metabolites(Liang et al., 2023). FTH1 is an intracellular iron-regulatory protein responsible for maintaining intracellular iron balance. Its expression decreases during ferroptosis, resulting in an increase in intracellular free iron ions(Liu et al., 2022). Quantitative PCR and western blotting had shown that celastrol significantly influenced intracellular oxidative stress and iron ion metabolism, leading to reduced ferroptosis in neuronal cells.

In our in vitro experiments, we initially determined the safe concentration of celastrol, ultimately selecting a drug concentration of 1μM for subsequent experiments. Morphological changes in OxyHb-injured neurones following treatment with different doses of celastrol demonstrated a protective effect on neurones, alleviating the damage caused by OxyHb. Compared with the OxyHb group, the celastrol-treated group displayed significantly decreased Fe2+, MDA, and SOD levels. Analysis of ferroptosis-related protein expression indicated reduced levels of ACSL4 and TFR1 and increased levels of GPX4 and FTH1. Collectively, these findings suggested a marked improvement in ICH following celastrol administration, highlighting its ability to inhibit ferroptosis and its consequent protective role against oxidative stress during anti-ICH injury interventions.

ACSL4 plays a central role in ICH-induced ferroptosis. We constructed an overexpression vector for ACSL4 (OE-ACSL4). Comparative analysis of the OxyHb+High and OE-ACSL4+OxyHb+High groups revealed a significant decrease in cell viability in the latter group, along with increased levels of Fe2+, MDA, and ROS. These results suggest that ACSL4 overexpression induces neuronal cell damage. Conversely, high doses of celastrol were found to suppress ACSL4 and TFR1 overexpression, while enhancing GPX4 and FTH1 expression, thus demonstrating neuroprotective effects. Subsequent qPCR and western blotting analyses supported these findings. Molecular docking studies revealed a direct interaction between celastrol and ACSL4. Taken together, these findings indicated that celastrol mitigated the harmful effects of ferroptosis on neurones, and alleviated ICH-induced cerebral damage by inhibiting ACSL4. The results of this study suggested that celastrol alleviated oxidative stress and promoted neurological recovery after stroke by suppressing ACSL4 expression during ferroptosis. These findings underscore the potential of celastrol as a therapeutic agent for the management of ICH. However, current investigations into the role of celastrol in combating ferroptosis are predominantly confined to cellular and animal studies, and clinical trials involving traditional Chinese medicine formulations and acupuncture are lacking. Although a few clinical trials using such formulations have validated the antiferroptotic effects of celastrol, the intricate nature of these formulations complicates the study of metabolic pathways and target actions. Moreover, in clinical scenarios, patients may present with complex conditions with traditional Chinese medicine components potentially eliciting diverse toxicological or physiological responses. Consequently, further exploration of the potential of traditional Chinese medicine to inhibit ferroptosis for ICH treatment holds significant promise in the development of traditional Chinese medicine -based therapies for ICH. Nonetheless, additional research leveraging advanced methodologies, such as network pharmacology, bioinformatics, molecular docking, and high-throughput mass spectrometry analysis, are still needed.

CRediT authorship contribution statement

Hengzhu Zhang: Writing – review & editing, Supervision, Project administration, Funding acquisition. **Zhengcun Yan:** Resources, Project administration, Conceptualization. **Yi Liu:** Writing – review & editing, Project administration, Investigation. **Min Wei:** Writing – original draft, Investigation, Funding acquisition, Conceptualization. **Yuping Li:** Writing – review & editing, Visualization, Supervision. **Xiaodong Wang:** Supervision, Investigation, Formal analysis. **Xingdong Wang:** Methodology, Investigation, Formal analysis. **Dongsheng Li:** Validation, Investigation, Formal analysis.

Conflicts of Interest

Our research was approved by Yangzhou University. The work described has been carried out in accordance with the National Institutes of Health – Office of Laboratory Animal Welfare policies and laws. All animal studies must comply with the ARRIVE guidelines. The ethics approval number was No. 202103467.Min Wei reports financial support was provided by National Natural Science Foundation of China (82301452) and Collaborative Integration of Traditional Chinese Medicine and Western Medicine (ZXXTGG2022C08). Hengzhu Zhang reports financial support was provided by Six One Project of Jiangsu Province (LGY2017026). If there are other authors, they declare that they have no known competing financial interests or personal relationships that could have appeared to influence the work reported in this paper.

References

Bai, Q., Xue, M., Yong, V.W., 2020. Microglia and macrophage phenotypes in intracerebral haemorrhage injury: therapeutic opportunities. Brain 143, 1297–1314.

Bonsack, F., Alleyne Jr., C.H., Sukumari-Ramesh, S., 2017. Resveratrol attenuates neurodegeneration and improves neurological outcomes after intracerebral hemorrhage in mice. Front Cell Neurosci. 11, 228.

Cao, Y., Li, Y., He, C., Yan, F., Li, J.R., Xu, H.Z., Zhuang, J.F., Zhou, H., Peng, Y.C., Fu, X. J., Lu, X.Y., Yao, Y., Wei, Y.Y., Tong, Y., Zhou, Y.F., Wang, L., 2021. Selective ferroptosis inhibitor liproxstatin-1 attenuates neurological deficits and neuroinflammation after subarachnoid hemorrhage. Neurosci. Bull. 37, 535–549.

Chen, M., Liu, M., Luo, Y., Cao, J., Zeng, F., Yang, L., Yang, J., Tao, T., Jiang, Y., 2022. Celastrol protects against cerebral ischemia/reperfusion injury in mice by inhibiting glycolysis through targeting HIF-1alpha/PDK1 Axis. Oxid. Med Cell Longev. 2022, 7420507.

Chow, A.M., Tang, D.W., Hanif, A., Brown, I.R., 2014. Localization of heat shock proteins in cerebral cortical cultures following induction by celastrol. Cell Stress Chaperon-.-. 19, 845–851.

Cui, Y., Zhang, Y., Zhao, X., Shao, L., Liu, G., Sun, C., Xu, R., Zhang, Z., 2021. ACSL4 exacerbates ischemic stroke by promoting ferroptosis-induced brain injury and neuroinflammation. Brain Behav. Immun. 93, 312–321.

Dixon, S.J., Lemberg, K.M., Lamprecht, M.R., Skouta, R., Zaitsev, E.M., Gleason, C.E., Patel, D.N., Bauer, A.J., Cantley, A.M., Yang, W.S., Morrison 3rd, B., Stockwell, B.R., 2012. Ferroptosis: an iron-dependent form of nonapoptotic cell death. Cell 149, 1060–1072.

Duan, L., Zhang, Y., Yang, Y., Su, S., Zhou, L., Lo, P.C., Cai, J., Qiao, Y., Li, M., Huang, S., Wang, H., Mo, Y., Wang, Q., 2021. Baicalin inhibits ferroptosis in intracerebral hemorrhage. Front Pharm. 12, 629379.

Fujii, J., Homma, T., Osaki, T., 2022. Superoxide radicals in the execution of cell death. Antioxidants 11.

Guan, Y., Cui, Z.J., Sun, B., Han, L.P., Li, C.J., Chen, L.M., 2016. Celastrol attenuates oxidative stress in the skeletal muscle of diabetic rats by regulating the AMPK-PGC1alpha-SIRT3 signaling pathway. Int J. Mol. Med 37, 1229–1238.

Haley, M.D., Gregson, B.A., Mould, W.A., Hanley, D.F., Mendelow, A.D., 2018. Retrospective methods analysis of semiautomated intracerebral hemorrhage volume quantification from a selection of the STICH II Cohort (Early Surgery Versus Initial Conservative Treatment in Patients With Spontaneous Supratentorial Lobar Intracerebral Haematomas). Stroke 49, 325–332.

Jia, J., Wang, Z., Zhang, M., Huang, C., Song, Y., Xu, F., Zhang, J., Li, J., He, M., Li, Y., Ao, G., Hong, C., Cao, Y., Chin, Y.E., Hua, Z.C., Cheng, J., 2020. SQR mediates therapeutic effects of H(2)S by targeting mitochondrial electron transport to induce mitochondrial uncoupling. Sci. Adv. 6 eaaz5752.

Jiang, M., Liu, X., Zhang, D., Wang, Y., Hu, X., Xu, F., Jin, M., Cao, F., Xu, L., 2018. Celastrol treatment protects against acute ischemic stroke-induced brain injury by promoting an IL-33/ST2 axis-mediated microglia/macrophage M2 polarization. J. Neuroinflamm. 15, 78.

Lan, T., Hu, L., Sun, T., Wang, X., Xiao, Z., Shen, D., Wu, W., Luo, Z., Wei, C., Wang, X., Liu, M., Guo, Y., Wang, L., Wang, Y., Lu, Y., Yu, Y., Yang, F., Zhang, C., Li, Q., 2023. H3K9 trimethylation dictates neuronal ferroptosis through repressing Tfr1. J. Cereb. Blood Flow. Metab. 43, 1365–1381.

Leclerc, J.L., Lampert, A.S., Loyola Amador, C., Schlakman, B., Vasilopoulos, T., Svendsen, P., Moestrup, S.K., Dore, S., 2018. The absence of the CD163 receptor has distinct temporal influences on intracerebral hemorrhage outcomes. J. Cereb. Blood Flow. Metab. 38, 262–273.

Li, Y., He, D., Zhang, X., Liu, Z., Zhang, X., Dong, L., Xing, Y., Wang, C., Qiao, H., Zhu, C., Chen, Y., 2012. Protective effect of celastrol in rat cerebral ischemia model: down-regulating p-JNK, p-c-Jun and NF-kappaB. Brain Res 1464, 8–13.

Li, Z., Li, Y., Han, J., Zhu, Z., Li, M., Liu, Q., Wang, Y., Shi, F.D., 2021. Formyl peptide receptor 1 signaling potentiates inflammatory brain injury. Sci. Transl. Med 13.

Liang, D., Feng, Y., Zandkarimi, F., Wang, H., Zhang, Z., Kim, J., Cai, Y., Gu, W., Stockwell, B.R., Jiang, X., 2023. Ferroptosis surveillance independent of GPX4 and differentially regulated by sex hormones. Cell 186, 2748–2764 e22.

Lin, M.W., Lin, C.C., Chen, Y.H., Yang, H.B., Hung, S.Y., 2019. Celastrol inhibits dopaminergic neuronal death of Parkinson's disease through activating mitophagy. Antioxidants 9.

Liu, N., Liang, Y., Wei, T., Zou, L., Huang, X., Kong, L., Tang, M., Zhang, T., 2022. The role of ferroptosis mediated by NRF2/ERK-regulated ferritinophagy in CdTe QDs-induced inflammation in macrophage. J. Hazard Mater. 436, 129043.

Liu, X., Nie, L., Zhang, Y., Yan, Y., Wang, C., Colic, M., Olszewski, K., Horbath, A., Chen, X., Lei, G., Mao, C., Wu, S., Zhuang, L., Poyurovsky, M.V., James You, M., Hart, T., Billadeau, D.D., Chen, J., Gan, B., 2023. Actin cytoskeleton vulnerability to disulfide stress mediates disulfidptosis. Nat. Cell Biol. 25, 404–414.

Liu, X., Olszewski, K., Zhang, Y., Lim, E.W., Shi, J., Zhang, X., Zhang, J., Lee, H., Koppula, P., Lei, G., Zhuang, L., You, M.J., Fang, B., Li, W., Metallo, C.M., Poyurovsky, M.V., Gan, B., 2020. Cystine transporter regulation of pentose phosphate pathway dependency and disulfide stress exposes a targetable metabolic vulnerability in cancer. Nat. Cell Biol. 22, 476–486.

Liu, X., Qi, K., Gong, Y., Long, X., Zhu, S., Lu, F., Lin, K., Xu, J., 2021. Ferulic acid alleviates myocardial ischemia reperfusion injury via upregulating AMPKalpha2 expression-mediated ferroptosis depression. J. Cardiovasc Pharm. 79, 489–500.

Luo, D., Zhao, J., Rong, J., 2016. Plant-derived triterpene celastrol ameliorates oxygen glucose deprivation-induced disruption of endothelial barrier assembly via inducing tight junction proteins. Phytomedicine 23, 1621–1628.

Pan, X., Zhao, Y., Cheng, T., Zheng, A., Ge, A., Zang, L., Xu, K., Tang, B., 2019. Monitoring NAD(P)H by an ultrasensitive fluorescent probe to reveal reductive stress induced by natural antioxidants in HepG2 cells under hypoxia. Chem. Sci. 10, 8179–8186.

Qin, Y., Liu, Y., Xiang, X., Long, X., Chen, Z., Huang, X., Yang, J., Li, W., 2023. Cuproptosis correlates with immunosuppressive tumor microenvironment based on pan-cancer multiomics and single-cell sequencing analysis. Mol. Cancer 22, 59.

Qu, X.F., Liang, T.Y., Wu, D.G., Lai, N.S., Deng, R.M., Ma, C., Li, X., Li, H.Y., Liu, Y.Z., Shen, H.T., Chen, G., 2021. Acyl-CoA synthetase long chain family member 4 plays detrimental role in early brain injury after subarachnoid hemorrhage in rats by inducing ferroptosis. CNS Neurosci. Ther. 27, 449–463.

Qu, X., Wang, N., Cheng, W., Xue, Y., Chen, W., Qi, M., 2019. MicroRNA-146a protects against intracerebral hemorrhage by inhibiting inflammation and oxidative stress. Exp. Ther. Med 18, 3920–3928.

Ren, S., Chen, Y., Wang, L., Wu, G., 2022. Neuronal ferroptosis after intracerebral hemorrhage. Front Mol. Biosci. 9, 966478.

Shi, K., Tian, D.C., Li, Z.G., Ducruet, A.F., Lawton, M.T., Shi, F.D., 2019. Global brain inflammation in stroke. Lancet Neurol. 18, 1058–1066.

Stockwell, B.R., Friedmann Angeli, J.P., Bayir, H., Bush, A.I., Conrad, M., Dixon, S.J., Fulda, S., Gascon, S., Hatzios, S.K., Kagan, V.E., Noel, K., Jiang, X., Linkermann, A., Murphy, M.E., Overholtzer, M., Oyagi, A., Pagnussat, G.C., Park, J., Ran, Q., Rosenfeld, C.S., Salnikow, K., Tang, D., Torti, F.M., Torti, S.V., Toyokuni, S., Woerpel, K.A., Zhang, D.D., 2017. Ferroptosis: a regulated cell death nexus linking metabolism, redox biology, and disease. Cell 171, 273–285.

Su, H., Peng, C., Liu, Y., 2024. Regulation of ferroptosis by PI3K/Akt signaling pathway: a promising therapeutic axis in cancer. Front Cell Dev. Biol. 12, 1372330.

Tsvetkov, P., Coy, S., Petrova, B., Dreishpoon, M., Verma, A., Abdusamad, M., Rossen, J., Joesch-Cohen, L., Humeidi, R., Spangler, R.D., Eaton, J.K., Frenkel, E., Kocak, M., Corsello, S.M., Lutsenko, S., Kanarek, N., Santagata, S., Golub, T.R., 2022. Copper induces cell death by targeting lipoylated TCA cycle proteins. Science 375, 1254–1261.

Wang, H., Lin, D., Yu, Q., Li, Z., Lenahan, C., Dong, Y., Wei, Q., Shao, A., 2021. A promising future of ferroptosis in tumor therapy. Front Cell Dev. Biol. 9, 629150.

Wu, G., Sun, S., Sheng, F., Wang, L., Wang, F., 2013. Perihematomal glutamate level is associated with the blood-brain barrier disruption in a rabbit model of intracerebral hemorrhage. Springerplus 2, 358.

Xu, H., Cai, Y., Yu, M., Sun, J., Cai, J., Li, J., Qin, B., Ying, G., Chen, T., Shen, Y., Jie, L., Xu, D., Gu, C., Wang, C., Hu, X., Chen, J., Wang, L., Chen, G., 2021. Celastrol protects against early brain injury after subarachnoid hemorrhage in rats through alleviating blood-brain barrier disruption and blocking necroptosis. Aging (Albany NY) 13, 16816–16833.

Yang, H., Ni, W., Jiang, H., Lei, Y., Su, J., Gu, Y., Zhou, L., 2018. Histone deacetylase inhibitor scriptaid alleviated neurological dysfunction after experimental intracerebral hemorrhage in mice. Behav. Neurol. 2018, 6583267.

Yang, Y., Zhu, T., Wang, X., Xiong, F., Hu, Z., Qiao, X., Yuan, X., Wang, D., 2022. ACSL3 and ACSL4, distinct roles in ferroptosis and cancers. Cancers (Basel) 14.

Zhang, Y., Geng, C., Liu, X., Li, M., Gao, M., Liu, X., Fang, F., Chang, Y., 2017. Celastrol ameliorates liver metabolic damage caused by a high-fat diet through Sirt1. Mol. Metab. 6, 138–147.

Zhang, C., Zhao, M., Wang, B., Su, Z., Guo, B., Qin, L., Zhang, W., Zheng, R., 2021b. The Nrf2-NLRP3-caspase-1 axis mediates the neuroprotective effects of Celastrol in Parkinson's disease. Redox Biol. 47, 102134.

Zhang, B., Zhong, Q., Chen, X., Wu, X., Sha, R., Song, G., Zhang, C., Chen, X., 2021a. Corrigendum: neuroprotective effects of celastrol on transient global cerebral ischemia rats via regulating HMGB1/NF-kappaB signaling pathway. Front Neurosci. 15, 637004.

Zhao, Q., Qi, T., 2023. The implications and prospect of cuproptosis-related genes and copper transporters in cancer progression. Front Oncol. 13, 1117164.

Zhu, Y., Liu, C., Sun, Z., 2015. Early combined therapy with pharmacologically induced hypothermia and edaravone exerts neuroprotective effects in a rat model of intracerebral hemorrhage. Cell Biochem Biophys. 73, 581–587.